International Journal of Nanomedicine

Dovepress
open access to scientific and medical research

Open Access Full Text Article

ORIGINAL RESEARCH

Dual effects and mechanism of TiO_2 nanotube arrays in reducing bacterial colonization and enhancing C3H10T1/2 cell adhesion

This article was published in the following Dove Press journal:
International Journal of Nanomedicine
13 August 2013
Number of times this article has been viewed

Zhaoxiang Peng[1,2,*]
Jiahua Ni[3,*]
Kang Zheng[2]
Yandong Shen[2]
Xiaoqing Wang[1]
Guo He[3]
Sungho Jin[4]
Tingting Tang[1]

[1]Shanghai Key Laboratory of Orthopaedic Implants, Department of Orthopaedic Surgery, Shanghai Ninth People's Hospital, Shanghai Jiaotong University School of Medicine, Shanghai, People's Republic of China; [2]Department of Orthopaedic Surgery, Ningbo Medical Treatment Center Lihuili Hospital, Ningbo, People's Republic of China; [3]State Key Lab of Metal Matrix Composites, School of Materials Science and Engineering, Shanghai Jiao Tong University, Shanghai, People's Republic of China; [4]Materials Science and Engineering, University of California, San Diego, La Jolla, CA, USA

*These authors contributed equally to this work

Abstract: Competition occurs between the osteoblasts in regional microenvironments and pathogens introduced during surgery, on the surface of bone implants, such as joint prostheses. The aim of this study was to modulate bacterial and osteoblast adhesion on implant surfaces by using a nanotube array. Titanium oxide (TiO_2) nanotube arrays, 30 nm or 80 nm in diameter, were prepared by a two-step anodization on titanium substrates. Mechanically polished and acid-etched titanium samples were also prepared to serve as control groups. The standard strains of *Staphylococcus epidermidis* (*S. epidermidis*, American Type Culture Collection [ATCC]35984) and mouse C3H10T1/2 cell lines with osteogenic potential were used to evaluate the different responses to the nanotube arrays, in bacteria and eukaryotic cells. We found that the initial adhesion and colonization of *S. epidermidis* on the surface of the TiO_2 nanotube arrays were significantly reduced and that the adhesion of C3H10T1/2 cells on the surface of the TiO_2 nanotube arrays was significantly enhanced when compared with the control samples. Based on a surface analysis of all four groups, we observed increased surface roughness, decreased water contact angles, and an enhanced concentration of oxygen and fluorine atoms on the TiO_2 nanotube surface. We conclude that the TiO_2 nanotube surface can reduce bacterial colonization and enhance C3H10T1/2 cell adhesion; multiple physical and chemical properties of the TiO_2 nanotube surface may contribute to these dual effects.

Keywords: bacterial adhesion, titanium implant, surface modification

Introduction

Titanium and titanium alloys have attracted tremendous attention for use in orthopedic and dental implants, due to their strong corrosion resistance, biocompatibility, low toxicity, and excellent mechanical properties.[1–4] However, material-related complications, such as aseptic loosening and infection continue to make orthopedic implant surgeries risky.[5] Aseptic loosening is the most common complication after joint replacement.[6,7] The gap between the implant and the surrounding bone tissues, caused by an unsuitable prosthetic surface for cell adhesion and poor osseointegration, is one of the primary causes of aseptic loosening.[8,9] The physical and chemical properties of the surface are known to be crucial for the ultimate interaction between the prosthesis and the biological system; however, the precise role of the surface chemistry and topography in the early stages of dental implant osseointegration remain poorly understood.[10] Recent studies have indicated that a nanostructure surface can enhance the adhesion, growth, and proliferation of osteoblasts compared with a traditional microstructure surface.[11–14] In addition, when the prosthesis is implanted in a human body, a blood-free area that is primarily composed of abraded particles and dead cell debris gradually forms at

Correspondence: Tingting Tang
Shanghai Key Laboratory of Orthopaedic Implants, Department of Orthopaedic Surgery, Shanghai Ninth People's Hospital, Shanghai Jiaotong University School of Medicine, 639 Zhizaoju Road, Shanghai 200011, People's Republic of China
Tel +86 21 2327 1133
Fax +86 21 6313 7020
Email tingtingtang@hotmail.com

Guo He
State Key Lab of Metal Matrix Composites, School of Materials Science and Engineering, Shanghai Jiao Tong University, 80 Dongchuan Road, Minhang District, Shanghai 200240, People's Republic of China
Tel +86 21 3420 2643
Fax +86 21 3420 2643
Email ghe@sjtu.edu.cn

the prosthesis–bone tissue interface. In this blood-free area, the innate immune system of the host is lost, and infection occurs easily.[15] Systemic antibiotics cannot reach this area, and thus, such infections are difficult to treat.[16] Hence, poor osseointegration around the prosthesis is also a risk factor for infection.[17,18]

Competition between cell adhesion and bacterial adhesion arises on prosthetic surfaces, and cell adhesion is inhibited when bacteria adhere more strongly than the cells, a notion that was first put forward by Gristina.[19] Adhered biofilm-positive bacteria irreversibly form into a biofilm,[20] and as a result of the physical protective effects of the biofilm matrix and the change in the bacterial metabolism, the antibiotic resistance of the biofilm bacteria will be 1,000 times stronger than that of normal bacteria.[21,22] Thus, inhibiting bacterial adhesion on the prosthesis surface at the initial stage of implantation is critical to preventing this type of infection. It is hence, necessary to improve the biological properties of prosthetic surfaces.

Most existing studies have focused on either promoting osteoblast activity or inhibiting bacterial adhesion, but no reported studies have considered both aspects. Hu et al found that immobilized vascular endothelial growth factor (VEGF) on titanium via heparin-VEGF interactions, can preserve the growth factor bioactivity on both osseous and vascular components and can concomitantly reduce bacterial infection.[23] Lee et al developed a novel gentamicin and bone morphogenic protein-2 for heparinized-titanium implants that enhanced osteoblast functions while simultaneously decreasing bacterial infections.[24] Shi et al found that the surface functionalization of titanium with carboxymethyl chitosan and immobilized bone morphogenetic protein-2 can provide a selective biointeractive surface that simultaneously enhances bone cell function and decreases bacterial adhesion.[25] Annunziata et al found that a titanium nitride coating significantly reduced bacterial adhesion and proliferation, while maintaining the prosthesis biological affinity for bone cell precursors.[26] We also found that the quaternary ammonium salt of chitosan is a potential material for coatings exhibiting both antibacterial and bone activity.[27–30]

Gong et al were the first to fabricate uniform titanium oxide (TiO_2) nanotube arrays, by in-situ anodization on the surface of titanium foil, in 2001.[31] TiO_2 nanotube arrays on the titanium surface can enhance osteoblast adhesion and proliferation,[32,33] and they are expected to be among the best choices for the surface modification of biomaterials due to their biocompatibility, cell growth enhancement, and unique nanotubular structures with tunable dimensions.[34,35] In recently published studies, many researchers have investigated the biomedical applications of TiO_2 nanotube arrays. To summarize some highlights, Bauer et al[36] used a TiO_2 nanotube array film as a bracket for the adhesion and proliferation of bone marrow mesenchymal stem cells; Popat et al[37] proposed the use of antibiotic-loaded TiO_2 nanotubes to inhibit bacterial adhesion; Roy et al[38] loaded drugs into TiO_2 nanotube arrays to control bleeding; Oh et al[32] found that stem cells can be regulated by TiO_2 nanotubes to generate particular cells. TiO_2 nanotube arrays are also likely to affect bacterial adhesion, with various results reported.[5,38,39] To date, as Neoh et al[40] have indicated, the vast majority of studies that have focused on the effects of surface topography on the response of bacteria and osteoblasts were carried out with either bacteria or osteoblasts, while the same substrate has not been assessed for both types of cells.

In this work, we aimed to develop an appropriate nanostructured surface for implants to simultaneously increase osteoblast adhesion and reduce the growth of pathogens. In this paper, TiO_2 nanotube arrays with different diameters were prepared by a two-step anodization on the titanium surface, and the responses of C3H10T1/2 cells and *Staphylococcus epidermidis* to the TiO_2 nanotube arrays were investigated and compared.

Materials and methods

Nanotube preparation

Titanium sheets (10 mm × 1 mm, 99.5% purity, annealed; Sh-puwei, Shanghai, People's Republic of China) were used as starting materials. The preparation process of the TiO_2 nanotube arrays was as follows: The sheets were degreased by ultrasonication in acetone, followed by a distilled water rinse. The samples were polished sequentially using #200, #600, #800, #1,000, and #1,500 abrasive papers (Golden Tiger sandpaper Co., Ltd., Hubei, People's Republic of China). The samples were chemically etched for 1 minute in a mixture of nitric acid (HNO_3) and hydrofluoric acid (HF) (1:1 volume/volume) immediately before anodization, to remove the native oxide film, followed by a distilled water rinse. Anodization was performed using a two-electrode configuration with a DC power supply. The electrolyte consisted of 0.6 volume% HF (96%) in water (H_2O), and a stainless steel sheet served as the cathode electrode. In this work, the applied voltages were 10 V and 20 V. Two-step anodization was used in this paper. For the first anodization step, one group of samples was anodized at 10 V for 10–15 minutes, while another group of samples was anodized at 20 V for 10–15 minutes. After the first anodization, all samples were chemically etched, for

1 minute, in a mixture of HNO_3 and HF, to remove the TiO_2 nanotube arrays formed in the first anodization step and were then washed with distilled water. Subsequently, these samples were immediately anodized again under the same conditions for the desired length of time: the group of samples anodized at 10 V during the first anodization step was anodized at 10 V for 45 minutes, whereas the applied voltage for the group of samples anodized at 20 V during the first step was fixed at 20 V for 45 minutes as the second anodization step. After the second anodization, all samples were thoroughly washed with distilled water and then dried by a stream of air.

In this work, apart from the TiO_2 nanotube arrays anodized at 10 V (group 1) and 20 V (group 2), another two groups of samples were prepared as control groups. For group 3, the titanium sheets were degreased by ultrasonication in acetone, followed by a distilled water rinse, and they were then polished sequentially using #200, #600, #800, #1,000, and #1,500 abrasive papers. For group 4, the titanium sheets were chemically etched for 10 minutes in a 0.6 volume% HF aqueous solution after degreasing and mechanical polishing. All experiments were conducted at room temperature.

Characterization

The surface morphologies and elemental compositions of all samples were observed by field emission scanning electron microscopy (SEM) (SIRION 200; FEI Co, Hillsboro, OR, USA) with an energy dispersive X-ray spectrometer (EDX) (INCA; Oxford Instruments, Abingdon, UK).

The surface roughness of all samples was measured by atomic force microscopy (AFM) (Nanoscope IV Multimode AFM; Veeco Instruments Ltd, Plainview, NY, USA). The measurements were conducted in ambient air under tapping mode, with a scan area of $2 \times 2\ \mu m^2$. The AFM data were analyzed using Nanoscope v7.20 software (Veeco Instruments Ltd).

To explore the wettability of the samples, the sessile drop method was used to obtain contact angle measurements from an optical contact angle measuring device (OCA20; DataPhysics Instruments GmbH, Filderstadt, Germany) with a camera. A 4 μL droplet of distilled water was dropped from the tip of a microliter syringe to the surface of the samples. After a period of 5 seconds had elapsed, the contact angle between the drop and the substrate was measured. Meanwhile, images were collected by the camera. At least five measurements at different spots were obtained for each specimen.

Bacteria culture

The standard American Type Culture Collection (ATCC)35984 strains (donated by Professor Qu Di, Molecular Virology Lab, Shanghai Medical College, Fudan University, People's Republic of China) consist of biofilm-positive *S. epidermidis*. The strains were stored in a medium containing 30% glycerol at −80°C. To obtain inocula for examination, the frozen ATCC35984 strains were incubated in tryptic soy agar (TSA) plates (Trypticase™; BD Biosciences, Franklin Lakes, NJ, USA) at 37°C under static culture conditions for 24 hours. Monoclonal strains were selected for use. These strains were incubated in 50 mL sterile glass tubes containing 10 mL tryptic soy broth (TSB, BD Biosciences) and were then placed on a rotary platform (130 rpm) at 37°C for 12 hours under aerobic conditions. After being dynamically cultured twice in fresh TSB media, the bacterial suspension was moved to a centrifuge tube and then centrifuged (8,000 g, 10 minutes). The supernatant was decanted, and the precipitate was diluted with fresh TSB media to a 1×10^7 colony forming units (CFU)/mL bacterial suspension.

Eukaryotic cell culture

Mouse C3H10T1/2 cell lines with osteogenic differentiation potential (provided by the Cell Bank of the Chinese Academy of Sciences, Shanghai, People's Republic of China) were cultured in Dulbecco's Modified Eagle's medium (DMEM; GIBCO, Grand Island, NY, USA) containing 10 volume% fetal bovine serum (FBS; Hyclone, Tauranga, New Zealand). The C3H10T1/2 cells were digested with 0.05% trypsin and 0.02% ethylenediaminetetraacetic acid (EDTA; GIBCO) when the cell density approached 90% confluence and were then subcultured at a 1:3 ratio. Once the cell density approached 90% confluence again, the C3H10T1/2 cells were digested with 0.05% trypsin and 0.02% EDTA, which was stopped by DMEM containing 10% fetal bovine serum, and the suspension was then diluted to 1×10^4 cells/mL.

Assay for bacterial adhesion and proliferation

The LIVE/DEAD® BacLight™ Bacterial Viability Kit (Molecular Probes® L7012, Life Technologies, Carlsbad, CA, USA) contains two fluorescent dyes: SYTO® 9 nucleic acid stain and propidium iodide (PI). The former causes live bacteria to emit green fluorescence, while the latter causes dead bacteria to emit red fluorescence, which can be used to differentiate between live and dead bacteria under a fluorescent microscope. According to the ratio given in the instructions (SYTO 9:PI:double distilled (dd)H_2O = 1.5 μL:1.5 μL:1 mL), the three types of solution were combined in a centrifuge tube and oscillated for thorough mixing. The operations above were performed while avoiding natural light.

Four groups of samples (10 mm × 1 mm) were placed in 12-well plates after autoclave sterilization. Then, 1.5 mL of a fresh bacterial suspension (1×10^7 CFU/mL) was placed into each individual well; the samples were then stored in an incubator for static culturing at 37°C. Each sample was removed by sterile tweezers after 1, 2, 3, 4, and 5 hours of cell culture and was rinsed lightly three times with phosphate-buffered saline (PBS) to remove nonadherent floating bacteria from the surface of the samples. Next, 200 μL of the fluorescent dye described above was dropped on each sample, and the samples were wrapped in aluminum foil for incubation without natural light at room temperature for 15 minutes. Confocal laser scanning microscopy (Leica TCS SP2; Leica Microsystems, Wetzlar, Germany) was used to observe the samples, and the data were statistically analyzed by WinSTAT® software (R Fitch Software, Stauffen, Germany).

Assay for cell adhesion, proliferation, and skeleton and adhesion proteins

4′,6-diamidino-2-phenylindole (DAPI) is a common fluorescent dye that can penetrate the cell membrane and combine with double-stranded DNA in the core, to mark the cell's position. The fluorescence generated by DAPI is 20 times brighter than the dye itself. A 1 mg/mL storage solution was prepared with ddH_2O, as described in the instruction manual, and the working fluid was diluted to 10 μg/mL using ddH_2O and stored at 4°C without natural light. Fluorescein isothiocyanate (FITC)-phalloidin (Sigma-Aldrich, St Louis, MO, USA) was used to stain F-actin, to indicate the cell skeleton. Four groups of samples were prepared as described above, with the cell concentration in each well, being approximately 1×10^5 cells/mL. Each condition was repeated three times, and the well plate was stored in an incubator under a 5% carbon dioxide (CO_2) environment.

The number of cells in each group of samples, after incubating for 1, 2, 8, 12, and 24 hours, was counted using the fluorescent dye. FITC-phalloidin was used to dye the F-actin, to indicate the cell skeleton, and DAPI was employed to dye the cell nucleus; further details have been reported by Coleman et al.[41,42] Adhesion plaque protein, also called vinculin, is a highly conserved cellular protein. This protein is related to the cell's adhesion and can connect to F-actin in other cells to form adhesion points between the cells and the substrate. Immunofluorescence staining of vinculin was performed using a 1:800 dilution of mouse Monoclonal Anti-Vinculin Antibody (Sigma-Aldrich); antibody labeling was performed via a 1:200 dilution of Alexa Fluor® 488 conjugated Goat Anti-Mouse immunoglobulin (Ig)G (Life Technologies), in accordance with the manufacturer's instructions. The samples were then viewed by confocal laser scanning microscopy (Leica TCS SP2).

Statistical analysis

Differences between groups were examined for statistical significance using an analysis of variance (ANOVA), presented as the mean (three independent experiments with each in duplicate, n = 3 per group) ± standard deviation. $P < 0.05$ was considered to indicate statistical significance.

Results

Physical and chemical properties of the different surfaces

Figure 1 shows the surface morphologies of the four groups of samples: mechanically polished titanium sheet (group 1); acid-etched titanium sheet (group 2); TiO_2 nanotube arrays anodized at 20 V (group 3); and TiO_2 nanotubes anodized at 10 V (group 4). The figure shows that regular grinding marks, incurred by mechanical processing, were present on the surface of the titanium sheet (group 1 in Figure 1); the grinding marks were irregular on the acid-etched titanium surface (group 2 in Figure 1). Highly ordered TiO_2 nanotube arrays were separately prepared by anodization at 20 V and 10 V. The average diameter of the TiO_2 nanotubes anodized at 20 V was approximately 80 nm (group 3 in Figure 1), and the average diameter of the TiO_2 nanotubes anodized at 10 V was approximately 30 nm (group 4 in Figure 1).

Figure 2 shows the EDX spectra of these four samples, and Table 1 shows their elemental composition. The titanium content was approximately 100% on the surface of the mechanically polished titanium. A small number of fluorine atoms (~0.95%) were detected on the surface of the acid-etched titanium. The TiO_2 nanotube arrays anodized at 10 V and 20 V had a similar elemental composition: the fluorine content was approximately 8%–9%, the oxygen content was ~50%, and the titanium content was ~40%. It is inferred that the fluorine detected on the surface of the TiO_2 nanotube arrays originated from residual electrolyte in the TiO_2 nanotubes.

AFM images of the surface morphologies of the four samples are shown in Figure 3, and the average surface roughness values measured by AFM are given in Table 2. According to the guidelines suggested for the topographic evaluation of implant surfaces by Wennerberg et al,[43] three parameters, including the mean roughness (roughness average), the root mean square roughness, and the maximum roughness depth, were used to evaluate the surface roughness of the samples.

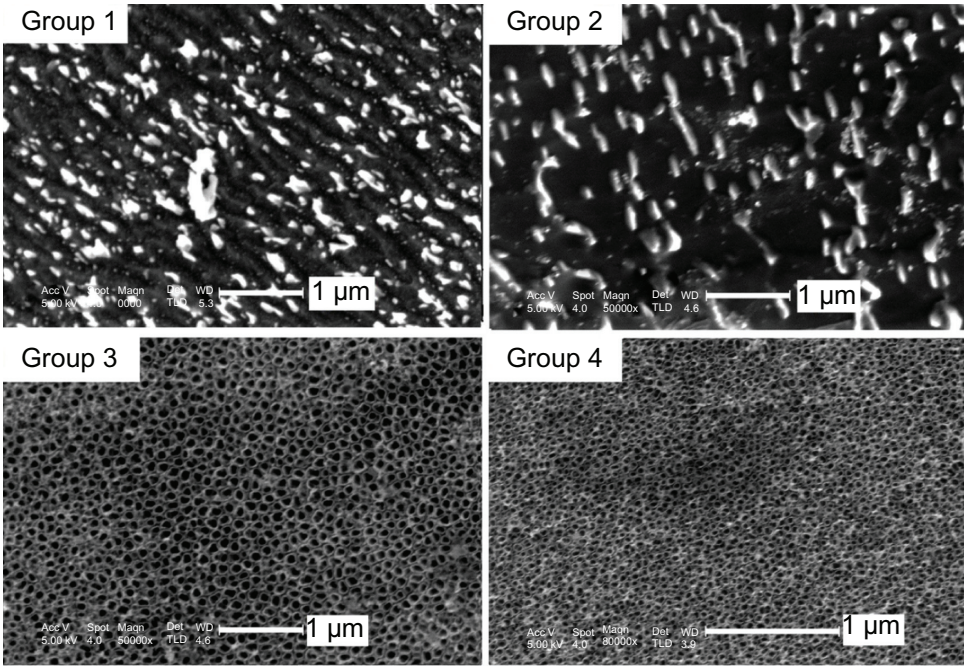

Figure 1 SEM images of the surface morphologies of the four groups: mechanically polished titanium sheet (group 1), acid-etched titanium sheet (group 2), TiO_2 nanotube arrays anodized at 20 V (group 3), and TiO_2 nanotube arrays anodized at 10 V (group 4).
Abbreviations: SEM, scanning electron microscopy; TiO_2, titanium oxide.

As indicated in Table 2, the surface of the TiO_2 nanotube arrays was rougher than that of the other two control groups of titanium. For the 80 nm diameter TiO_2 nanotube arrays, the average roughness and root mean square roughness were higher than for the others, but the maximum roughness depth of the 80 nm TiO_2 nanotube arrays (479.53 ± 8.356 nm) was slightly lower than that of the 30 nm TiO_2 nanotube arrays (536.54 ± 10.240 nm).

Figure 4 shows the water contact angle images, and Table 1 lists the average contact angle for the four groups.

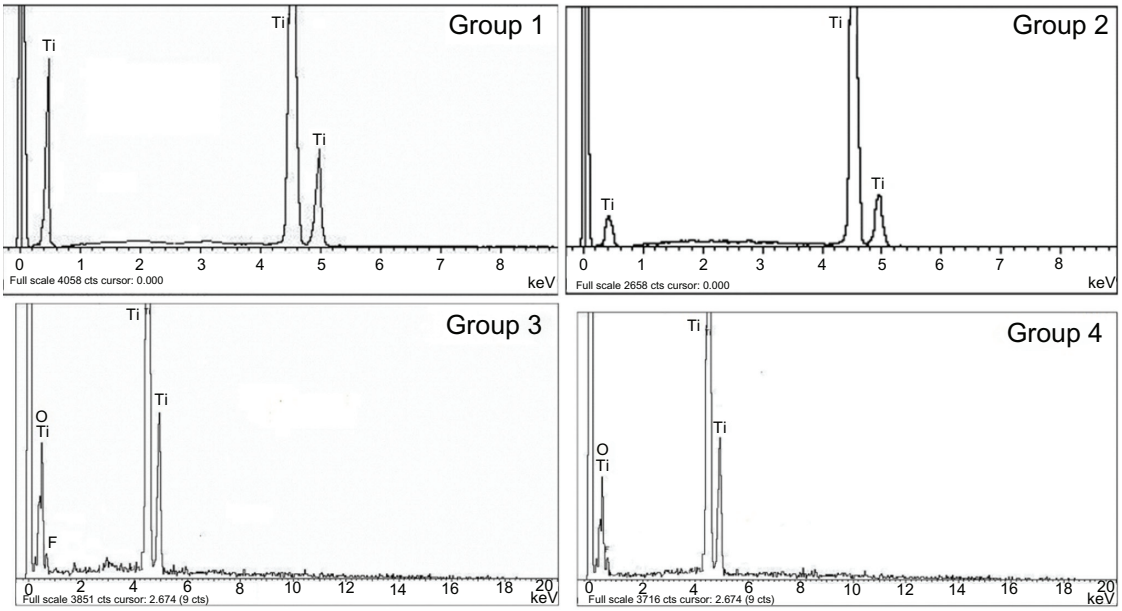

Figure 2 EDX spectra of the four groups, including the mechanically polished titanium sheet (group 1), acid-etched titanium sheet (group 2), TiO_2 nanotube arrays anodized at 20 V (group 3), and TiO_2 nanotube arrays anodized at 10 V (group 4).
Abbreviations: EDX, energy dispersive X-ray; TiO_2, titanium oxide.

Table 1 The relationship between the elemental composition, surface roughness, and water contact angle of the four groups and their biological activities

	Group 1	Group 2	Group 3	Group 4
O element (atomic %)	0	0	48.63 ± 4.43	52.04 ± 5.02
F element (atomic %)	0	0.95 ± 1.78	9.16 ± 1.46	8.32 ± 2.92
Roughness (means ± standard deviation)	12.996 ± 1.034	26.177 ± 1.970	54.996 ± 0.453	42.667 ± 2.304
Water contact angle (°)	73.3 ± 5.7	55.8 ± 4.3	24.5 ± 5.2	33.9 ± 3.7
Cytoskeletal proteins	No significant difference			
Vinculin expression	None	Weak	Strong	Moderate
The living bacteria per cm^2 (5 hours)	2.12×10^8	1.34×10^8	2.15×10^7	5.70×10^7
Adhered osteogenic cells per cm^2 (24 hours)	7.02×10^4	8.15×10^4	1.20×10^5	9.55×10^4

The largest water contact angle was ~75°, on the surface of the titanium sheet. The contact angle on the acid-etched titanium sheet was ~55°, and the angle reached ~34° for the group 4 samples. The lowest contact angle was observed for the group 3 samples, approaching 25°. It is obvious that the contact angles of the TiO_2 nanotube arrays were much lower than those of the titanium and acid-etched titanium sheets, which implies that the TiO_2 nanotube arrays significantly improved the wettability of the sample surface.

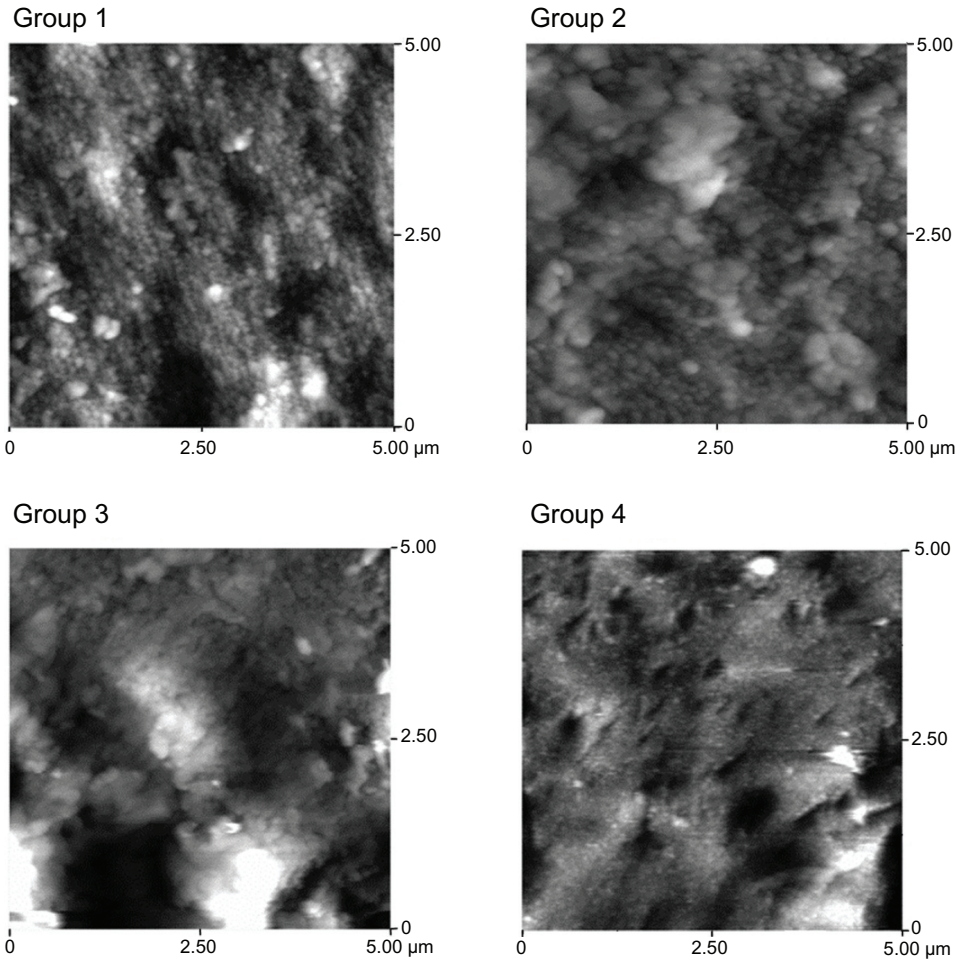

Figure 3 AFM images of the surface roughness of the four groups: mechanically polished titanium sheet (group 1), acid-etched titanium sheet (group 2), TiO_2 nanotube arrays anodized at 20 V (group 3), and TiO_2 nanotube arrays anodized at 10 V (group 4).
Abbreviations: AFM, atomic force microscopy; TiO_2, titanium oxide.

Table 2 The surface roughness of the four groups

	Ra (nm)	Rq (nm)	Rmax (nm)
Group 1	10.116 ± 2.062	12.999 ± 1.034	106.53 ± 5.790
Group 2	20.744 ± 3.682	26.177 ± 1.970	194.81 ± 4.872
Group 3	39.120 ± 2.960	54.996 ± 0.453	479.53 ± 8.356
Group 4	31.052 ± 2.203	42.667 ± 2.304	536.54 ± 10.240

Note: Figures are mean ± standard deviation.
Abbreviations: Ra, average roughness; Rq, root mean square roughness; Rmax, maximum roughness depth.

Bacterial adhesion and proliferation on the different surfaces

Three views of each sample were randomly selected for imaging by a confocal laser scanning microscope (Figure 5), which were then quantified by the accessory software. Green fluorescence indicated live bacteria, while red fluorescence indicated dead bacteria. From Figure 5, it is clear that live bacteria on the TiO_2 nanotube arrays were greatly inhibited at each time point compared with the titanium sheets. Statistical analysis (Figure 6) showed that both the total and live bacteria on the TiO_2 nanotube arrays were much lower than on the mechanically polished titanium ($P < 0.05$) at each time point (after 1, 2, 3, 4, and 5 hours of incubation) or on the acid-etched titanium at 2 hours ($P < 0.05$). Furthermore, the levels of total and live bacteria on the 80 nm TiO_2 nanotubes were lower than on the 30 nm TiO_2 nanotubes at 2 hours ($P < 0.05$).

C3H10T1/2 cell adhesion on the different surfaces

The adhesion of C3H10T1/2 cells for these four groups is shown in Figure 7. With increasing culture time, the cells gradually spread and grew to confluence on the surface. Three views of each group sample were randomly selected, and the cell numbers, as indicated by blue dots (stained with DAPI), were counted per square centimeter. As shown in Figure 8, the cell density on the 30 nm and 80 nm TiO_2 nanotube arrays was obviously higher than that on the mechanically polished and acid-etched titanium sheets ($P < 0.01$), and the cell density on the 80 nm TiO_2 nanotube arrays was remarkably higher than that of the other groups at 2, 8, 12, and 24 hours.

Cell spreading and vinculin expression on the different surfaces

Figure 9 shows a single cell spreading on the surface, with immunofluorescent blue staining of the nucleus, red cytoskeletal F-actin fibers, and green adhered vinculin.

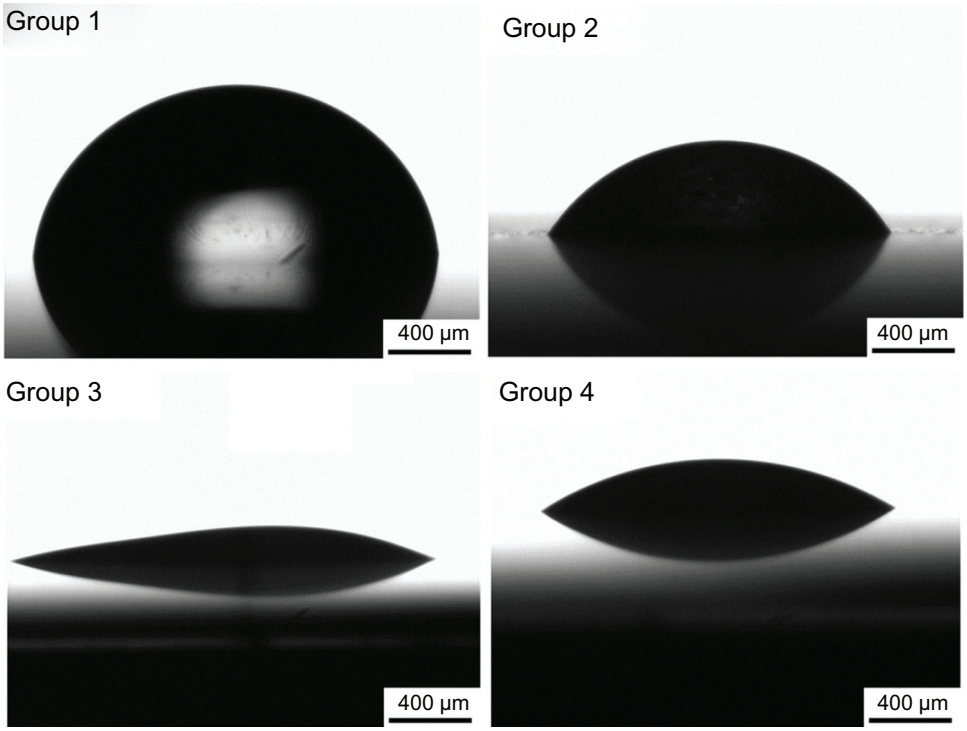

Figure 4 Schematic of the water contact angle for the four groups: mechanically polished titanium sheet (group 1), acid-etched titanium sheet (group 2), TiO_2 nanotube arrays anodized at 20 V (group 3), and TiO_2 nanotube arrays anodized at 10 V (group 4).
Abbreviation: TiO_2, titanium oxide.

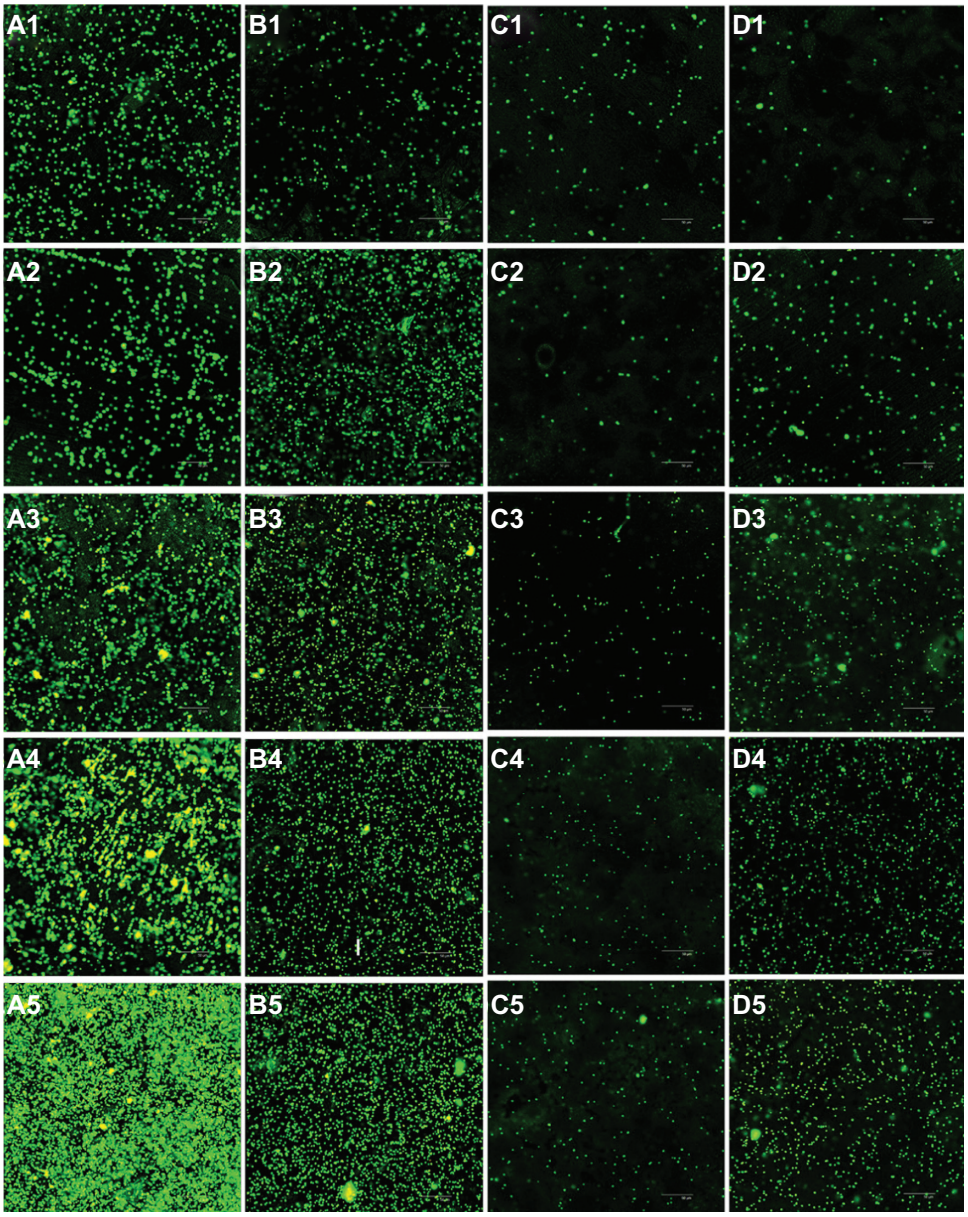

Figure 5 Confocal laser scanning microscopy analysis of *Staphylococcus epidermidis* colonies on mechanically polished titanium (**A**), acid-etched titanium (**B**), 80 nm TiO_2 nanotube arrays (**C**), and 30 nm TiO_2 nanotube arrays (**D**), after 1 hour (**1**), 2 hours (**2**), 3 hours (**3**), 4 hours (**4**), and 5 hours (**5**) of incubation (400×).

Vinculin is the principal protein in adhesion plaque, and its expression indirectly reflects the cell's adhesion strength on a material's surface. We observed brighter staining of vinculin in the cell skeleton on the TiO_2 nanotube surface than on the surface of the mechanically polished or acid-etched titanium after a 24-hour incubation.

Discussion

The eukaryotic cells (ie, osteoblasts) and bacteria utilized in this study displayed different growth patterns on the implant surface. The eukaryotic cells grew on the surface with contact inhibition, while the bacteria lived on the surface as an aggregate. The adhesion mechanisms of eukaryotic cells and bacteria on the surface also differed; the adhesion of eukaryotic cells mainly depended on the formation of adhesion plaque,[40] while the bacterial membrane played an important role in bacterial adhesion to surfaces.[44] It is known that appropriately sized nanotubes promote the formation of osteoblast adhesion plaque proteins by increasing osteoblast adhesion.[45–47] Here, we further demonstrated that the surface of TiO_2 nanotube arrays has the dual function of reducing bacterial colonization and enhancing C3H10T1/2 cell adhesion.

Many reports have demonstrated that nanosurfaces can promote the adhesion, proliferation and differentiation of

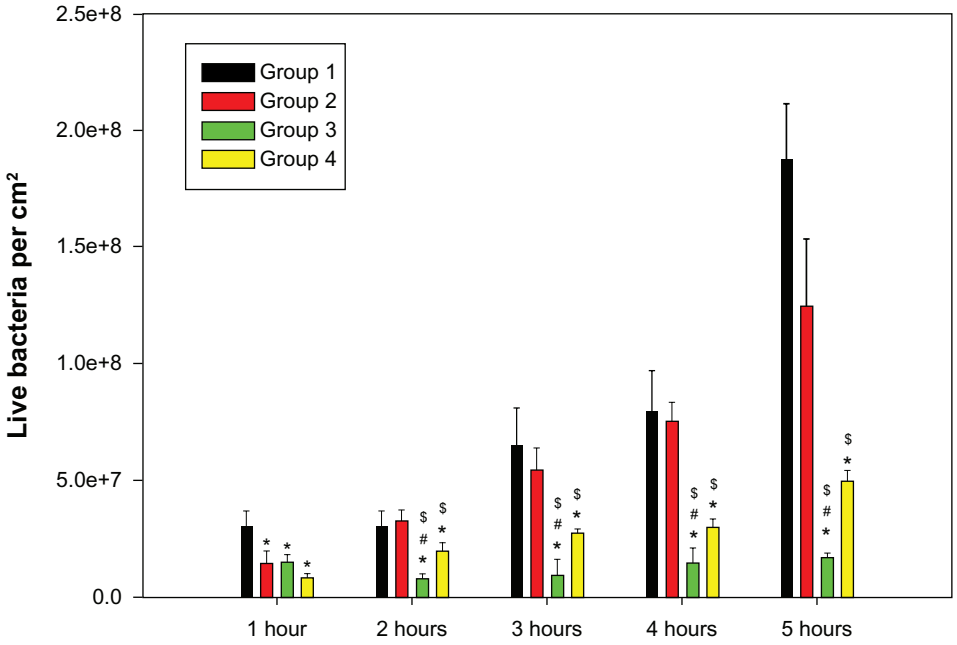

Figure 6 A comparison of live *Staphylococcus epidermidis* on the titanium surfaces of the four groups, including pure titanium (group 1), acid-etched titanium (group 2), and nanotube titanium (group 3 and group 4), after 1, 2, 3, 4, and 5 hours of incubation.
Notes: e+8 means $\times 10^8$; $^*P < 0.05$ compared with group 1; $^\#P < 0.05$ compared with group 4; $^\$P < 0.05$ compared with group 2.

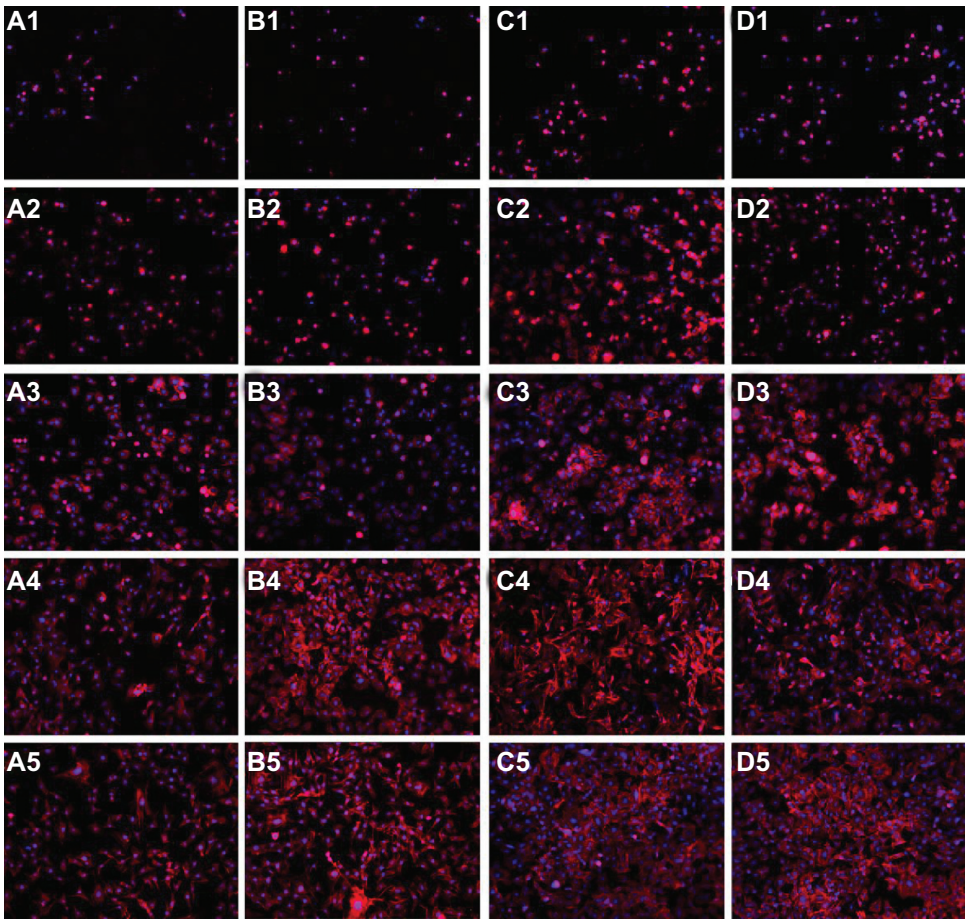

Figure 7 C3H10T1/2 cell growth on mechanically polished titanium (**A**), acid-etched titanium (**B**), 80 nm TiO_2 nanotube arrays (**C**), and 30 nm TiO_2 nanotube arrays (**D**), after 1 hour (**1**), 2 hours (**2**), 8 hours (**3**), 12 hours (**4**), and 24 hours (**5**) of incubation.
Note: The cells were fluorescently stained for cytoskeletal F-actin fibers (red) and at the nucleus (blue) (100×).

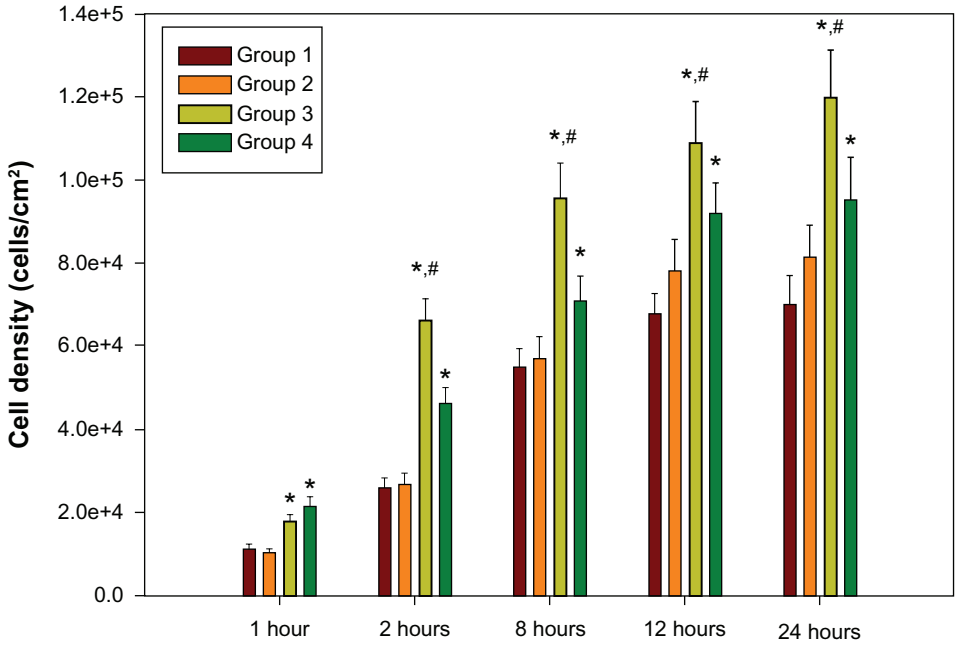

Figure 8 C3H10T1/2 cell growth on TiO_2 nanotube arrays (group 3 and group 4) compared with mechanically polished titanium (group 1) and acid-etched titanium (group 2) after 2 hours, 8 hours, 12 hours, and 24 hours of cell culture.
Notes: e+8 means $\times 10^8$; $^*P < 0.05$ compared with titanium; $^{\#}P < 0.05$ compared with group 4.

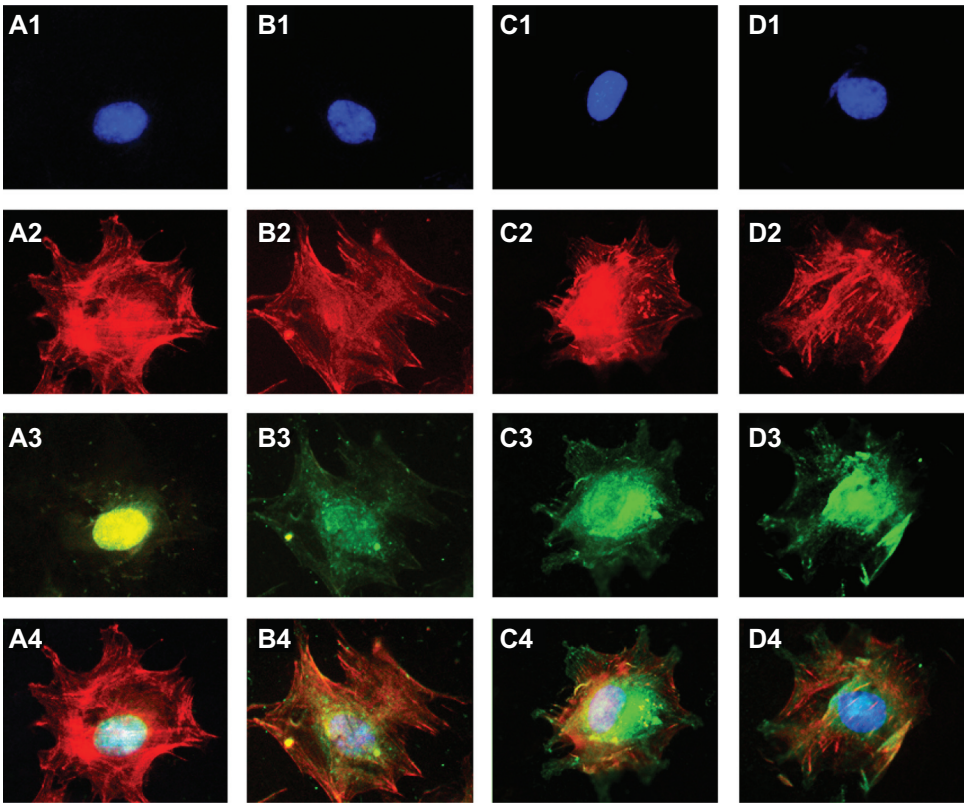

Figure 9 C3H10T1/2 cells were fluorescently stained after a 24-hour culture period on mechanically polished titanium (**A**), acid-etched titanium (**B**), 80 nm TiO_2 nanotube arrays (**C**), and 30 nm TiO_2 nanotube arrays (**D**).
Notes: The blue nucleus is indicated in (**1**), the red cytoskeletal F-actin fibers are indicated in (**2**), the green adhered protein vinculin is indicated in (**3**), and the merged images are shown in (**4**) (400×).

osteogenic progenitors,[48–51] but there have been varied results regarding bacterial adhesion. Colon et al[39] compared the behavior of *S. epidermidis* and osteoblasts on nanostructured and microstructured zinc oxide (ZnO) and TiO_2. They found that *S. epidermidis* adhesion on nanostructured ZnO and TiO_2 was weaker than that observed with microphage formulations. Puckett et al found that compared with smooth titanium nanosurfaces, rough titanium nanosurfaces decreased the bacterial adherence, while nanotubular and nanotextured titanium increased the bacterial attachment. They also reported that anodized surfaces (nanotubular and nanotextured titanium) decreased the percentage of living cells compared with nonfluorinated surfaces (nanorough and conventional titanium).[5] Popat et al observed that TiO_2 nanotubes loaded with the antibiotic gentamicin significantly reduced bacterial adhesion.[37] We argue that these varied results may be related to the complex physical and chemical changes that occur on different nanosurfaces.

Pathogens that cause infections in orthopedic implants include the *Staphylococcus* genus, the Enterobacteriaceae family, the *Pseudomonas* genus, the *Enterococcus* genus, etc. In this paper, we chose *S. epidermidis* to investigate bacteria growth on a nanotube surface. According to reports from Arciola et al and Campoccia et al,[52,53] *Staphylococcus* has been implicated in 66%−75.5% of severe orthopedic implant-related infections. While these researchers confirmed the importance of *Staphylococcus* as the most prevalent cause of infection, their data indicated an unexpectedly high prevalence, of 42% and 44%, of *S. epidermidis* in infected hip and knee arthroprostheses, respectively. Considering the common adhesion mechanism of the different types of bacteria on the implant surface, the results observed for *S. epidermis* may translate to other species of bacteria as well.

In this study, we also explored how the TiO_2 nanotube surface could be altered to modulate the response of osteogenic progenitors or bacteria. As indicated in Table 1, the physical characteristics and chemical compositions differed among the four groups. The nanotube surface (80 nm or 30 nm in diameter) had an increased roughness and decreased water contact angles, as well as a high concentration of oxygen and fluorine atoms, which may have been induced by the preparation process. The presence of oxygen has been reported to be advantageous for biological activity.[54] Although some reports have found that fluorine can enhance bacterial adhesion on the surface of biomaterials,[55,56] others have reported that fluorine shows antibacterial ability.[57,58]

Our data indicate that the roughness of both TiO_2 nanotube surfaces was higher than that of the two control samples. We also found that the water contact angles on both TiO_2 nanotube surfaces, especially on the surface of the 80 nm TiO_2 nanotubes, were much lower than those of the two control groups, indicating that the TiO_2 nanotube surfaces had improved hydrophilic performance. It is inferred that suspensions of C3H10T1/2 cells or bacteria on a TiO_2 nanotube surface will spread and disperse over a larger area than on a non-nanosurface. It is known that cell spreading can promote the proliferation and differentiation of C3H10T1/2 cells, while the separation of bacteria may prevent bacteria communication and colonization. Vinculin is a key focal adhesion protein that can stabilize the talin−integrin complex and increase cell adhesion. Cells can stably adhere to the surface, activating the expression of vinculin.[59–61] Hence, vinculin expression on the prosthesis can reflect, to some extent, the cell adhesion strength. In this study, we noted stronger vinculin immunostaining for the TiO_2 nanotube surfaces than for the two control groups, which may be attributed to the increased adherence of C3H10T1/2 cells.

Conclusion

In summary, the initial adhesion and growth of *S. epidermidis* on the surface of TiO_2 nanotube arrays were inhibited, especially on the 80 nm TiO_2 nanotube arrays. Meanwhile, the adhesion of C3H10T1/2 cells on the surface of the TiO_2 nanotube arrays was enhanced. The observed dual effects of the nanotube surface likely result from multiple factors, including both physical characteristics (higher surface roughness and lower water contact angle) and chemical composition (higher concentration of oxygen and fluorine).

Acknowledgments

This research was supported by a grant from the National Natural Science Foundation of China (31271015), the Program for Key Disciplines of the Shanghai Municipal Education Commission (J50206), the continuing support program for the Shu-guang scholars of the Shanghai Municipal Education Commission, and Programs Supported by the Ningbo Natural Science Foundation (2012A610223, 2012C50001).

Disclosure

The authors report no conflicts of interest in this work.

References

1. Long M, Rack HJ. Titanium alloys in total joint replacement – a materials science perspective. *Biomaterials*. 1998;19(18):1621–1639.

2. Ekelund JA, Lindquist LW, Carlsson GE, Jemt T. Implant treatment in the edentulous mandible: a prospective study on Brånemark system implants over more than 20 years. *Int J Prosthodont*. 2003;16(6):602–608.
3. Ferrigno N, Laureti M, Fanali S, Grippaudo G. A long-term follow-up study of non-submerged ITI implants in the treatment of totally edentulous jaws. Part I: Ten-year life table analysis of a prospective multicenter study with 1286 implants. *Clin Oral Implants Res*. 2002;13(3):260–273.
4. Bigerelle M, Anselme K, Noël B, Ruderman I, Hardouin P, Iost A. Improvement in the morphology of Ti-based surfaces: a new process to increase in vitro human osteoblast response. *Biomaterials*. 2002;23(7):1563–1577.
5. Puckett SD, Taylor E, Raimondo T, Webster TJ. The relationship between the nanostructure of titanium surfaces and bacterial attachment. *Biomaterials*. 2010;31(4):706–713.
6. Carr AJ, Robertsson O, Graves S, et al. Knee replacement. *Lancet*. 2012;379:1331–1340.
7. Milošev I, Kovač S, Trebše R, Levašič V, Pišot V. Comparison of ten-year survivorship of hip prostheses with use of conventional polyethylene, metal-on-metal, or ceramic-on-ceramic bearings. *J Bone Joint Surg Am*. 2012;94(19):1756–1763.
8. Drees P, Eckardt A, Gay RE, Gay S, Huber LC. Mechanisms of disease: Molecular insights into aseptic loosening of orthopedic implants. *Nat Clin Pract Rheumatol*. 2007;3(3):165–171.
9. Bordini B, Stea S, De Clerico M, Strazzari S, Sasdelli A, Toni A. Factors affecting aseptic loosening of 4750 total hip arthroplasties: multivariate survival analysis. *BMC Musculoskelet Disord*. 2007;8:69.
10. Le Guéhennec L, Soueidan A, Layrolle P, Amouriq Y. Surface treatments of titanium dental implants for rapid osseointegration. *Dent Mater*. 2007;23(7):844–854.
11. Yun KD, Yang Y, Lim HP, et al. Effect of nanotubular-micro-roughened titanium surface on cell response in vitro and osseointegration in vivo. *Mater Sci Eng C*. 2010;30(1):27–33.
12. Okada S, Ito H, Nagai A, Komotori J, Imai H. Adhesion of osteoblast-like cells on nanostructured hydroxyapatite. *Acta Biomater*. 2010;6(2):591–597.
13. Mendonça G, Mendonça DB, Aragão FJ, Cooper LF. Advancing dental implant surface technology – from micron- to nanotopography. *Biomaterials*. 2008;29(28):3822–3835.
14. Annunziata M, Oliva A, Buosciolo A, Giordano M, Guida A, Guida L. Bone marrow mesenchymal stem cell response to nano-structured oxidized and turned titanium surfaces. *Clin Oral Implants Res*. 2012;23(6):733–740.
15. Zimmerli W, Moser C. Pathogenesis and treatment concepts of orthopaedic biofilm infections. *FEMS Immunol Med Microbiol*. 2012;65(2):158–168.
16. Moran E, Byren I, Atkins BL. The diagnosis and management of prosthetic joint infections. *J Antimicrob Chemother*. 2010;65 Suppl 3:iii45–iii54.
17. Lindhe J, Meyle J; Group D of European Workshop on Periodontology. Peri-implant diseases: Consensus Report of the Sixth European Workshop on Periodontology. *J Clin Periodontol*. 2008;35(Suppl 8):282–285.
18. Mombelli A, van Oosten MA, Schurch E, Land NP. The microbiota associated with successful or failing osseointegrated titanium implants. *Oral Microbiol Immunol*. 1987;2(4):145–151.
19. Gristina AG. Biomaterial-centered infection: microbial adhesion versus tissue integration. *Science*. 1987;237(4822):1588–1595.
20. Ariza J, Euba G, Murillo O. Infecciones relacionadas con las prótesis articulares. [Orthopedic device-related infections.] *Enferm Infect Microbiol Clin*. 2008;26(6):380–390. Spanish.
21. Cerca N, Martins S, Cerca F, et al. Comparative assessment of antibiotic susceptibility of coagulase-negative staphylococci in biofilm versus planktonic culture as assessed by bacterial enumeration or rapid XTT colorimetry. *J Antimicrob Chemother*. 2005;56(2):331–336.
22. Fux CA, Costerton JW, Stewart PS, Stoodley P. Survival strategies of infectious biofilms. *Trends Microbiol*. 2005;13(1):34–40.
23. Hu X, Neoh KG, Zhang J, Kang ET, Wang W. Immobilization strategy for optimizing VEGF's concurrent bioactivity towards endothelial cells and osteoblasts on implant surfaces. *Biomaterials*. 2012;33(32):8082–8093.
24. Lee DW, Yun YP, Park K, Kim SE. Gentamicin and bone morphogenic protein-2 (BMP-2)-delivering heparinized-titanium implant with enhanced antibacterial activity and osteointegration. *Bone*. 2012;50(4):974–982.
25. Shi Z, Neoh KG, Kang ET, Poh CK, Wang W. Surface functionalization of titanium with carboxymethyl chitosan and immobilized bone morphogenetic protein-2 for enhanced osseointegration. *Biomacromolecules*. 2009;10(6):1603–1611.
26. Annunziata M, Oliva A, Basile MA, et al. The effects of titanium nitride-coating on the topographic and biological features of TPS implant surfaces. *J Dent*. 2011;39(11):720–728.
27. Peng ZX, Wang L, Du L, Guo SR, Wang XQ, Tang TT. Adjustment of the antibacterial activity and biocompatibility of hydroxypropyltrimethyl ammonium chloride chitosan by varying the degree of substitution of quaternary ammonium. *Carbohydr Polym*. 2010;81(2):275–283.
28. Peng ZX, Tu B, Shen Y, et al. Quaternized chitosan inhibits icaA transcription and biofilm formation by Staphylococcus on a titanium surface. *Antimicrob Agents Chemother*. 2011;55(2):860–866.
29. Tan H, Peng Z, Li Q, Xu X, Guo S, Tang T. The use of quaternised chitosan-loaded PMMA to inhibit biofilm formation and downregulate the virulence-associated gene expression of antibiotic-resistant staphylococcus. *Biomaterials*. 2012;33(2):365–377.
30. Tan H, Guo S, Yang S, Xu X, Tang T. Physical characterization and osteogenic activity of the quaternized chitosan-loaded PMMA bone cement. *Acta Biomater*. 2012;8(6):2166–2174.
31. Gong D, Grimes CA, Varghese OK, et al. Titanium oxide nanotube arrays prepared by anodic oxidation. *J Mater Res*. 2001;16(12):3331–3334.
32. Oh S, Brammer KS, Li YS, et al. Stem cell fate dictated solely by altered nanotube dimension. *Proc Natl Acad Sci U S A*. 2009;106(7):2130–2135.
33. Eaninwene G, Yao C, Webster TJ. Enhanced osteoblast adhesion to drug-coated anodized nanotubular titanium surfaces. *Int J Nanomedicine*. 2008;3(2):257–264.
34. Crawford GA, Chawla N. Porous hierarchical TiO2 nanostructures: processing and microstructure relationships. *Acta Mater*. 2009;57(3):854–867.
35. von Wilmowsky C, Bauer S, Lutz R, et al. In vivo evaluation of anodic TiO2 nanotubes: an experimental study in the pig. *J Biomed Mater Res Part B Appl Biomater*. 2009;89(1):165–171.
36. Bauer S, Park J, von der Mark K, Schmuki P. Improved attachment of mesenchymal stem cells on super-hydrophobic TiO2 nanotubes. *Acta Biomater*. 2008;4(5):1576–1582.
37. Popat KC, Eltgroth M, Latempa TJ, Grimes CA, Desai TA. Decreased Staphylococcus epidermis adhesion and increased osteoblast functionality on antibiotic-loaded titania nanotubes. *Biomaterials*. 2007;28(32):4880–4888.
38. Roy SC, Paulose M, Grimes CA. The effect of TiO2 nanotubes in the enhancement of blood clotting for the control of hemorrhage. *Biomaterials*. 2007;28(31):4667–4672.
39. Colon G, Ward BC, Webster TJ. Increased osteoblast and decreased Staphylococcus epidermidis functions on nanophase ZnO and TiO2. *J Biomed Mater Res A*. 2006;78(3):595–604.
40. Neoh KG, Hu X, Zheng D, Kang ET. Balancing osteoblast functions and bacterial adhesion on functionalized titanium surfaces. *Biomaterials*. 2012;33(10):2813–2822.
41. Coleman AW, Maguire MJ, Coleman JR. Mithramycin- and 4′-6-diamidino-2-phenylindole (DAPI)-DNA staining for fluorescence microspectrophotometric measurement of DNA in nuclei, plastids, and virus particles. *J Histochem Cytochem*. 1981;29(8):959–968.
42. Spudich A. Immunolabeling of cells grown attached to a substratum or in suspension with actin antibodies. *Cold Spring Harb Protoc*. 2011;2011(9):pii.

43. Wennerberg A, Albrektsson T. Suggested guidelines for the topographic evaluation of implant surfaces. *Int J Oral Maxillofac Implants*. 2000;15(3):331–344.
44. Anselme K, Davidson P, Popa AM, Giazzon M, Liley M, Ploux L. The interaction of cells and bacteria with surfaces structured at the nanometre scale. *Acta Biomater*. 2010;6(10):3824–3846.
45. Nel AE, Mädler L, Velegol D, et al. Understanding biophysicochemical interactions at the nano-bio interface. *Nat Mater*. 2009;8(7):543–557.
46. Park J, Bauer S, Schlegel KA, Neukam FW, von der Mark K, Schmuki P. TiO2 nanotube surfaces: 15 nm – an optimal length scale of surface topography for cell adhesion and differentiation. *Small*. 2009;5(6):666–671.
47. Gongadze E, Kabaso D, Bauer S, et al. Adhesion of osteoblasts to a nanorough titanium implant surface. *Int J Nanomedicine*. 2011;6:1801–1816.
48. Tan J, Saltzman WM. Biomaterials with hierarchically defined micro- and nanoscale structure. *Biomaterials*. 2004;25(17):3593–3601.
49. Zhang W, Li Z, Liu Y, et al. Biofunctionalization of a titanium surface with a nano-sawtooth structure regulates the behavior of rat bone marrow mesenchymal stem cells. *Int J Nanomedicine*. 2012;7:4459–4472.
50. Brammer KS, Oh S, Cobb CJ, Bjursten LM, van der Heyde H, Jin S. Improved bone-forming functionality on diameter-controlled TiO(2) nanotube surface. *Acta Biomater*. 2009;5(8):3215–3223.
51. Guida L, Annunziata M, Rocci A, Contaldo M, Rullo R, Oliva A. Biological response of human bone marrow mesenchymal stem cells to fluoride-modified titanium surfaces. *Clin Oral Implants Res*. 2010;21(11):1234–1241.
52. Arciola CR, An YH, Campoccia D, Donati ME, Montanaro L. Etiology of implant orthopedic infections: a survey on 1027 clinical isolates. *Int J Artif Organs*. 2005;28(11):1091–1100.
53. Campoccia D, Montanaro L, Arciola CR. The significance of infection related to orthopedic devices and issues of antibiotic resistance. *Biomaterials*. 2006;27(11):2331–2339.
54. Park JY, Gemmell CH, Davies JE. Platelet interactions with titanium: modulation of platelet activity by surface topography. *Biomaterials*. 2001;22(19):2671–2682.
55. Katsikogianni M, Spiliopoulou I, Dowling DP, Missirlis YF. Adhesion of slime producing Staphylococcus epidermidis strains to PVC and diamond-like carbon/silver/fluorinated coatings. *J Mater Sci Mater Med*. 2006;17(8):679–689.
56. Li B, Logan BE. Bacterial adhesion to glass and metal-oxide surfaces. *Colloids Surf B Biointerfaces*. 2004;36(2):81–90.
57. Nurhaerani, Arita K, Shinonaga Y, Nishino M. Plasma-based fluorine ion implantation into dental materials for inhibition of bacterial adhesion. *Dent Mater J*. 2006;25(4):684–692.
58. Shinonaga Y, Arita K. Antibacterial effect of acrylic dental devices after surface modification by fluorine and silver dual-ion implantation. *Acta Biomater*. 2012;8(3):1388–1393.
59. Hu K, Ji L, Applegate KT, Danuser G, Waterman-Storer CM. Differential transmission of actin motion within focal adhesions. *Science*. 2007;315(5808):111–115.
60. Critchley DR, Holt MR, Barry ST, Priddle H, Hemmings L, Norman J. Integrin-mediated cell adhesion: the cytoskeletal connection. *Biochem Soc Symp*. 1999;65:79–99.
61. Chen Y, Dokholyan NV. Insights into allosteric control of vinculin function from its large scale conformational dynamics. *J Biol Chem*. 2006;281(39):29148–29154.